Transp Porous Med (2009) 79:1–14
DOI 10.1007/s11242-008-9233-9

# Anisotropy of Seismic Attenuation in Fractured Media: Theory and Ultrasonic Experiment

**T. I. Chichinina · I. R. Obolentseva · G. Ronquillo-Jarillo**

Received: 31 January 2008 / Accepted: 1 April 2008 / Published online: 25 April 2008


**Abstract** This is a study on anisotropy of seismic attenuation in a transversely isotropic (TI) model, which is a long-wavelength equivalent of an isotropic medium with embedded parallel fractures. The model is based on Schoenberg's linear-slip theory. Attenuation is introduced by means of a complex-valued stiffness matrix, which includes complex-valued normal and tangential weaknesses. To study the peculiarities of seismic attenuation versus wave-propagation direction in TI media, numerical modeling was performed. The model-input data were the complex-valued weaknesses found from the laboratory ultrasonic experiment made with a Plexiglas plate-stack model, oil-saturated (wet) and air-filled (dry). The laboratory experiment and the numerical modeling have shown that in the vicinity of the symmetry axis, in the wet model, P-wave attenuation is close to S-wave attenuation, while in the dry model, P-wave attenuation is much greater than S-wave attenuation. Moreover, the fluid fill affects the P-wave attenuation pattern. In the dry (air-saturated) model, the attenuation pattern in the vicinity of the symmetry axis exhibits steeper slope and curvature than in the wet (oil-saturated) model. To define the slope or the curvature, a QVO gradient was introduced, which was found to be proportional to the symmetry-axis $Q_S/Q_P$-ratio, which explains the differences between dry and wet models. Thus, depending on the $Q_S/Q_P$-ratio, the QVO gradient can serve as an indicator of the type of fluid in fractures, because the QVO gradient is greater in gas-saturated than in liquid-saturated rocks. The analysis of P-wave attenuation anisotropy in seismic reflection and vertical seismic profiling data can be useful in seismic exploration for distinguishing gas from water in fractures.

**Keywords** Q-anisotropy · Attenuation · Seismic anisotropy · Fractures · Ultrasonic experiment · Transversely isotropic (TI) medium · Linear-slip model · Seismic quality factor $Q$ versus offset (QVO) · $Q_S/Q_P$-ratio

T. I. Chichinina (✉) · G. Ronquillo-Jarillo
Instituto Mexicano del Petroleo, Eje Central Lazaro Cardenas 152, Mexico D.F. 07730, Mexico
e-mail: tchichin@imp.mx

I. R. Obolentseva
Institute of Petroleum Geology and Geophysics of Siberian Branch of Russian Academy of Sciences, Koptyug Prospect 3, Novosibirsk 630090, Russia

## 1 Introduction

Azimuthal anisotropy of attenuation due to vertical fracturing of rocks attracts considerable interest because it shows promise in seismic exploration for hydrocarbon-bearing rocks. Liu et al. (1993), MacBeth (1999), Clark et al. (2001), Chapman (2003), Vasconcelos and Jenner (2005), Varela et al. (2006), Chichinina et al. (2006a,b), Maultzsch et al. (2007), Liu et al. (2007) reveal different aspects of this problem.

In the present work, we concentrate our efforts on a so far untouched topic—consideration of the attenuation anisotropy for all three wave types (P, SV, SH) with a sequential aim of joint inversion of such data for solving the practical problems related to search for hydrocarbons. The problem is examined for a TI medium, which is an effective model of rocks with parallel fractures. Solution of the inverse problem in explicit form requires deriving approximate expressions for the attenuation functions. Parameterization of the attenuation functions can be quite different depending on geological and rock-physics conditions involving attenuation mechanisms. Because these factors are as a rule poorly known, an effective-medium model for describing attenuation in fractured rocks must be reasonably general.

Among all elastic models describing parallel fracturing of rocks, the most general and relatively simple is Schoenberg's TI including fracture compliances, or weaknesses, as they are named by Bakulin et al. (2000). This model is based on the linear-slip theory and serves as a long-wave equivalent of a fractured rock with one fracture set (Schoenberg 1980, 1983; Schoenberg and Douma 1988; Schoenberg and Sayers 1995). For this reason, we introduce anisotropic attenuation into this model. Schoenberg's formulations are indistinguishable from those of Hudson (1981), if appropriate values of normal and tangential weaknesses are selected. In Hudson's model, the effect of attenuation is modeled by complex-valued elastic constants (Hudson et al. 1996, 2001).

In the previous work (Chichinina et al. 2007a,b), we began to develop the formalism for complex-valued stiffnesses in terms of an LS TI model with a vertical symmetry axis (VTI LS), using complex-valued weaknesses instead of real ones in Schoenberg's stiffness matrix. To verify the validity of this formalism, we used data on velocities and attenuation of P- and S-waves from the laboratory ultrasonic experiment of Gik and Bobrov (1996); the data were fitted by theoretical functions for LS TI model. The experiment was completed using two states of the model: dry and oil-saturated. The present work continues these studies and seeks to ascertain the attenuation attributes depending both on P- and S-waves that could help to distinguish between dry and saturated rocks. Such an attribute appears to be the QVO gradient depending on the $Q_S/Q_P$-ratio at the symmetry axis.

## 2 Theoretical Effective Model for Attenuation in Fractured Rocks

In seismic studies, a formation containing sets of parallel fractures can be approximated with a homogeneous anisotropic medium if fracture spacings are much less than seismic wavelengths (see, for example, (Bakulin et al. 2000)). The most general effective model of rocks with one set of parallel fractures is Schoenberg's TI based on LS theory (Schoenberg 1980, 1983). Fractures are described by linear-slip interfaces, which are characterized by normal and tangential weaknesses (these are the dimensionless parameters $\Delta_N$ and $\Delta_T$ that are within the limits (0, 1)). To transform Schoenberg's elastic model into the attenuative (viscoelastic) model, we replace the real-valued weaknesses $\Delta_N$ and $\Delta_T$ by complex-valued $\tilde{\Delta}_N$ and $\tilde{\Delta}_T$. Then the stiffness matrix given by Hsu and Schoenberg (1993, p. 967) acquires the following form (note that it is a VTI medium, with vertical symmetry axis $z$):

$$\widetilde{\mathrm{C}}=\begin{bmatrix} M\left(1-\xi^2\widetilde{\Delta}_N\right) & \lambda\left(1-\xi\widetilde{\Delta}_N\right) & \lambda\left(1-\widetilde{\Delta}_N\right) & 0 & 0 & 0 \\ \lambda\left(1-\xi\widetilde{\Delta}_N\right) & M\left(1-\xi^2\widetilde{\Delta}_N\right) & \lambda\left(1-\widetilde{\Delta}_N\right) & 0 & 0 & 0 \\ \lambda\left(1-\widetilde{\Delta}_N\right) & \lambda\left(1-\widetilde{\Delta}_N\right) & M\left(1-\widetilde{\Delta}_N\right) & 0 & 0 & 0 \\ 0 & 0 & 0 & \mu\left(1-\widetilde{\Delta}_N\right) & 0 & 0 \\ 0 & 0 & 0 & 0 & \mu\left(1-\widetilde{\Delta}_N\right) & 0 \\ 0 & 0 & 0 & 0 & 0 & \mu \end{bmatrix}. \quad (1)$$

where $M = \lambda + 2\mu$ and $\xi = \lambda/M$. $\tilde{\Delta}_\mathrm{N}$ and $\tilde{\Delta}_\mathrm{T}$ are complex-valued normal (index N) and tangential (index T) weaknesses,

$$\tilde{\Delta}_\mathrm{N} \equiv \Delta_\mathrm{N} - i\,\Delta_\mathrm{N}^\mathrm{I}, \quad \tilde{\Delta}_\mathrm{T} \equiv \Delta_\mathrm{T} - i\,\Delta_\mathrm{T}^\mathrm{I}, \quad (2)$$

$\lambda$ and $\mu$ are the Lame's constants of an isotropic background rock (or material),

$$\mu = \rho V_\mathrm{S}^2, \quad \lambda + 2\mu = \rho V_\mathrm{P}^2 \quad , \quad (3)$$

$V_\mathrm{S}$ and $V_\mathrm{P}$ are S- and P-wave velocities in the background, and $\rho$ is the density of the background.

The form of the stiffness matrix $\tilde{C}$ implies that we assume that the background rock is not attenuative ($\lambda$ and $\mu$ are real-valued) and that all attenuation occurs within fractures, which are characterized by complex-valued weaknesses $\tilde{\Delta}_\mathrm{N}$ and $\tilde{\Delta}_\mathrm{T}$. In doing so, we facilitate solution of the problem, although all calculations could be made with complex-valued $\lambda$ and $\mu$.

The attenuation $Q^{-1}$, i.e., the inverse quality factor $Q$, can be defined (see, e.g., Crampin 1981; Carcione 2000) as

$$Q_\mathrm{m}^{-1}(\alpha) = \mathrm{Im}\,\tilde{V}_\mathrm{m}^2(\alpha)/Re\,\tilde{V}_\mathrm{m}^2(\alpha), \quad (4)$$

where index m (m = P, SV, SH) means P-, SV-, and SH-waves, and $\tilde{V}_\mathrm{m}^2(\alpha)$ is complex-valued squared phase velocity versus wave-propagation direction $\alpha$. A wave normal $\boldsymbol{n}\,(\sin\alpha, 0, \cos\alpha)$ makes an angle $\alpha$ with the symmetry axis $z$ of VTI medium. Three complex-valued velocities $\tilde{V}_\mathrm{m}^2(\alpha)$, m = P, SV, SH, were derived as complex-valued eigenvalues of the Christoffel tensor $\tilde{C}_{ijkl}\,n_j n_l \rho^{-1}$,

$$\tilde{V}_\mathrm{P}^2(\alpha) = V_\mathrm{P}^2[1 - \tilde{\Delta}_\mathrm{N}(1 - 2g\sin^2\alpha)^2 - \tilde{\Delta}_\mathrm{T} g \sin^2 2\alpha], \quad (5)$$

$$\tilde{V}_\mathrm{SV}^2(\alpha) = V_\mathrm{S}^2[1 - \tilde{\Delta}_\mathrm{T} - (g\tilde{\Delta}_\mathrm{N} - \tilde{\Delta}_\mathrm{T})\sin^2 2\alpha], \quad (6)$$

$$\tilde{V}_\mathrm{SH}^2(\alpha) = V_\mathrm{S}^2(1 - \tilde{\Delta}_\mathrm{T}\cos^2\alpha), \quad (7)$$

where $\tilde{\Delta}_\mathrm{N}$ and $\tilde{\Delta}_\mathrm{T}$ are given by (2), and $g = \mu/(\lambda + 2\mu) = (V_\mathrm{S}/V_\mathrm{P})^2$. Note that for an elastic medium with real-valued $\Delta_\mathrm{N}$ and $\Delta_\mathrm{T}$, the expressions for $V_\mathrm{m}^2(\alpha)$ look like Eqs. 5–7 and were derived by Schoenberg and Douma (1988, p. 581).

Substitution of (5)–(7) into (4) yields the attenuation $Q_\mathrm{m}^{-1}(\alpha)$ of P-, SV-, and SH-waves:

$$Q_\mathrm{P}^{-1}(\alpha) = \frac{\Delta_\mathrm{N}^\mathrm{I}(1 - 2g\sin^2\alpha)^2 + \Delta_\mathrm{T}^\mathrm{I} g \sin^2 2\alpha}{1 - \Delta_\mathrm{N}(1 - 2g\sin^2\alpha)^2 - \Delta_\mathrm{T} g \sin^2 2\alpha}, \quad (8)$$

$$Q_{\mathrm{SH}}^{-1}(\alpha) = \frac{\Delta_{\mathrm{T}}^{\mathrm{I}} \cos^2 \alpha}{1 - \Delta_{\mathrm{T}} \cos^2 \alpha}, \tag{9}$$

$$Q_{\mathrm{SV}}^{-1}(\alpha) = \frac{\Delta_{\mathrm{T}}^{\mathrm{I}} + \left(g\Delta_{\mathrm{N}}^{\mathrm{I}} - \Delta_{\mathrm{T}}^{\mathrm{I}}\right) \sin^2 2\alpha}{1 - \Delta_{\mathrm{T}} - (g\Delta_{\mathrm{N}} - \Delta_{\mathrm{T}}) \sin^2 2\alpha}. \tag{10}$$

The imaginary parts $\Delta_{\mathrm{N}}^{\mathrm{I}}$ and $\Delta_{\mathrm{T}}^{\mathrm{I}}$ of the weaknesses (2) can be related to physical parameters (e.g., fluid viscosity, rock permeability, porosity, etc.) differentiating attenuation caused by either attenuation mechanism. For example, the mechanism due to local fluid flows during seismic wave propagation in a medium containing aligned microcracks in an equal-porosity background is described by complex-valued functions (Hudson et al. 1996), which can be related to complex-valued normal and tangential weaknesses. Chichinina et al. (2006a,b) used a similar approach to compute and analyze azimuthal variations of attenuation due to vertical fractures with gas, oil, or brine embedded within a porous rock.

Note that actually Eqs. 8–10 give only the anisotropic parts of the attenuations for P-, SH- and SV-waves. The complete attenuations are the sums of the attenuation in the isotropic background rock ($Q_{\mathrm{b}}^{-1}$) and the attenuation due to parallel fractures ($Q_{\mathrm{f}}^{-1}$):

$$Q_{\Sigma}^{-1}(\alpha) = Q_{\mathrm{b}}^{-1} + Q_{\mathrm{f}}^{-1}(\alpha), \tag{11}$$

where the isotropic part of the attenuation, ($Q_{\mathrm{b}}^{-1}$), is a directionally independent quantity, $Q_{\mathrm{b}}^{-1} = \mathrm{const}$, and the anisotropic part of attenuation, $Q_{\mathrm{f}}^{-1}(\alpha)$, is a function of wave propagation direction $\alpha$ given by Eqs. 8–10. The P-wave attenuation in the background, $Q_{\mathrm{b}}^{-1}$, can be defined as $(Q_{\mathrm{b}}^{-1})_{\mathrm{P}} = \mathrm{Im}\tilde{V}_{\mathrm{b,P}}/Re\tilde{V}_{\mathrm{b,P}}$, and the S-wave attenuation as $(Q_{\mathrm{b}}^{-1})_{\mathrm{S}} = \mathrm{Im}\tilde{V}_{\mathrm{b,S}}/Re\tilde{V}_{\mathrm{b,S}}$, where $\tilde{V}_{\mathrm{b,P}}$ and $\tilde{V}_{\mathrm{b,S}}$ are the complex-valued velocities in the background; they can be defined from complex-valued Lame's constants $\tilde{\lambda}$ and $\tilde{\mu}$ for the background, by analogy with Eq. 3, as $\tilde{V}_{\mathrm{b,P}}^2 = (\tilde{\lambda} + 2\tilde{\mu})/\rho$ and $\tilde{V}_{\mathrm{b,S}}^2 = \tilde{\mu}/\rho$. Thus, we reduce the problem to the calculation of anisotropic attenuation $Q_{\mathrm{f}}^{-1}(\alpha)$ with subsequent addition of the constant attenuation from the background, $Q_{\mathrm{b}}^{-1}$, following Eq. 11.

## 3 Linear Approximations for P-, SV-, SH-wave Attenuations

In the range $\alpha = 0$–$40°$, the expressions (8)–(10) for the attenuations can be approximated, with a sufficient accuracy, by linear functions of $\sin^2 \alpha$ (or $\sin^2 2\alpha$ in the case of the SV-wave):

$$Q_{\mathrm{P}}^{-1}(\alpha) \approx A + B \sin^2 \alpha, \tag{12}$$

where

$$A = \frac{\Delta_{\mathrm{N}}^{\mathrm{I}}}{(1 - \Delta_{\mathrm{N}})} \equiv Q_{\mathrm{P}\perp}^{-1}, \quad B = \frac{4g\left[(1 - \Delta_{\mathrm{N}})\Delta_{\mathrm{T}}^{\mathrm{I}} - (1 - \Delta_{\mathrm{T}})\Delta_{\mathrm{N}}^{\mathrm{I}}\right]}{(1 - \Delta_{\mathrm{N}})^2}; \tag{13}$$

$$Q_{\mathrm{SH}}^{-1}(\alpha) \approx A_{\mathrm{S}} + B_{\mathrm{SH}} \sin^2 \alpha, \tag{14}$$

$$Q_{\mathrm{SV}}^{-1}(\alpha) \approx A_{\mathrm{S}} + B_{\mathrm{SV}} \sin^2 2\alpha, \tag{15}$$

with

$$A_{\mathrm{S}} = \Delta_{\mathrm{T}}^{\mathrm{I}}/(1 - \Delta_{\mathrm{T}}) \equiv Q_{\mathrm{S}\perp}^{-1}, \quad B_{\mathrm{SH}} = -\Delta_{\mathrm{T}}^{\mathrm{I}}/(1 - \Delta_{\mathrm{T}})^2,$$
$$B_{\mathrm{SV}} = \left[\Delta_{\mathrm{N}}^{\mathrm{I}}(1 - \Delta_{\mathrm{T}})g - \Delta_{\mathrm{T}}^{\mathrm{I}}(1 - \Delta_{\mathrm{N}}g)\right]/(1 - \Delta_{\mathrm{T}})^2.$$

Note that for the complete incidence-angle range, $\alpha = 0$–$90°$, the P-wave attenuation should be approximated by the three-term function

$$Q_{\mathrm{P}}^{-1}(\alpha) \approx A + B \sin^2\alpha + C \sin^4\alpha, \tag{16}$$

where

$$C = \Delta_{\mathrm{N}}^{\mathrm{I}}\left[4g\frac{g(1+3\Delta_{\mathrm{N}}+4\Delta_{\mathrm{T}}^2)-\Delta_{\mathrm{T}}[1+4g-\Delta_{\mathrm{N}}(1-4g)]}{(1-\Delta_{\mathrm{N}})^3}\right] - \Delta_{\mathrm{T}}^{\mathrm{I}}\left[4g\frac{1-\Delta_{\mathrm{N}}(1-4g)-4g\Delta_{\mathrm{T}}}{(1-\Delta_{\mathrm{N}})^2}\right];$$

the coefficients $A$ and $B$ are given by Eq. 13.

The approximations are useful for interpretation of experimental data. In seismic exploration, the linear approximation for P-wave attenuation, Eq. 12, can be used in reflection data for an analysis of attenuation versus $\sin^2\alpha$ (or offset), which should be estimated in each trace of common-mid-point (CMP) gathered before stacking.

## 4 Laboratory Ultrasonic Experiment

Laboratory ultrasonic experiments measuring attenuation anisotropy, caused by oriented fractures, cracks, clay particles, etc., are conducted using different samples, natural and artificial, along with models. For example, attenuation anisotropy has been studied in rock samples (Domnesteanu et al. 2002; Shi and Deng 2005; Best et al. 2007), composite samples with certain geometries of aligned cracks (Hosten et al. 1987; Sothcott et al. 2007), and plate-stack models (Gik and Bobrov 1996; Zhu et al. 2007). From all these models, the most suitable for us (i.e., of correspondence to the VTI LS model) is the Plexiglas plate-stack model of Gik and Bobrov (1996). We use the data on velocities and attenuations from this work in a quantitative analysis. It should be noted that the lucite plate-stack model of Hsu and Schoenberg (1993) is closely similar to that of Gik and Bobrov (1996). Hsu and Schoenberg (1993), studying a behavior of velocities in their model, proved the full validity of the LS theory in an elastic medium. We do the same, but in terms of a viscoelastic medium (LS model with attenuation) while studying both velocities and attenuations.

As for correspondence between the field and the laboratory ultrasonic experiment data, the similarity principle holds. It is supposed that $V_{\mathrm{field}}/V_{\mathrm{model}} = 1$, $\rho_{\mathrm{field}}/\rho_{\mathrm{model}} = 1$, where $V_{\mathrm{field}}$ and $\rho_{\mathrm{field}}$ are velocity and density in the Earth model (field data), and $V_{\mathrm{model}}$ and $\rho_{\mathrm{model}}$ are velocity and density in the experiment (in the Plexiglas model). In the experiment, the dominant pulse frequency was $f_{\mathrm{model}} = 100\,\mathrm{kHz}$, then the wave length $\lambda_{\mathrm{model}} = V/f_{\mathrm{model}} \cong 2.8\,\mathrm{km\,s^{-1}}/10^5\,\mathrm{s^{-1}} = 28\,\mathrm{mm}$. For field parameters, for example, at the frequency $f_{\mathrm{field}} = 28\,\mathrm{Hz}$, this means the wave length $\lambda_{\mathrm{field}} = V/f_{\mathrm{field}} \cong 2.8\,\mathrm{km\,s^{-1}}/28\,\mathrm{s^{-1}} = 0.1\,\mathrm{km}$. In the experiment, the fracture spacing (the plate thickness) is equal to 1 mm, which is $0.04\,\lambda_{\mathrm{model}}$. This corresponds to the fracture spacing 4 m in the Earth model. The fracture opening in the experiment was 0.001 mm; this corresponds to the fracture opening 3.6 mm in the Earth model. Thus,

$$\text{seismic wavelength} >> \text{fracture spacing} >> \text{fracture opening};$$

this is according to the constraint for Schoenberg's linear-slip model (see, for example, (Bakulin et al. 2000)).

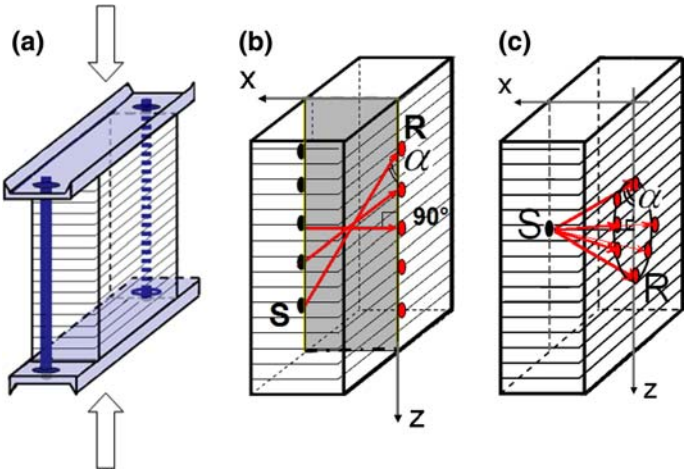


**Fig. 1** Scheme of ultrasonic experiment performed by Gik and Bobrov (1996). Uniaxial pressure is applied by means of two screws and holder of two steel plates (**a**). The location of the sources (S) and receivers (R) in the linear acquisition system (**b**), and the conical acquisition system (**c**). The angle $\alpha$ is the wave-propagation angle between the ray and the symmetry axis $z$ of VTI model

The model of Gik and Bobrov (1996) consists of rectangular Plexiglas plates, each 1 mm thick and $72 \times 250\,\text{mm}^2$, used to imitate a fractured medium with parallel fractures; the height of the model is 250 mm. The plates are held together under uniaxial pressure applied to the top and the bottom of the model. Technically, it was done by placing the model into a holder of two steel plates which were fastened by means of screws as shown in Fig. 1a. The greater sides of the model, $250 \times 250\,\text{mm}^2$, were used for placing sources and receivers. The ultrasonic experiment was performed in two configurations (b and c shown in Fig. 1), representing "linear" and "conical" acquisition system.

In the linear acquisition system shown in Fig. 1b, sources (S) are located on one side of the model and receivers (R) on the other, so the rays SR move toward the shaded plane. In the conical acquisition system in Fig. 1c, all the rays from the source S toward the receivers R form a cone. In both cases, the location of each source-receiver pair can be given by the angle $\alpha$ between the ray and the vertical axis $z$ normal to fracture planes.

The $\alpha$-angle interval available in the experiment was not larger than $(25°, 90°)$ in the linear acquisition system and $(45°, 90°)$ in the conical acquisition system due to the model size and acquisition geometry. In both acquisition systems, $\max \alpha = 90°$ since the corresponding rays are horizontal. The angle $\alpha = 0°$ and the angles in its locality are inaccessible because the top and the bottom of the model are covered with the steel plates shown in Fig. 1a.

The attenuation $Q^{-1}$ and velocities $V$ of P-, SV-, and SH-waves were estimated under each source-receiver pair, i.e., each angle $\alpha$. The experiment was performed for two states: oil-filled ("wet model") and air-filled ("dry model"). We fit the experimental data by theoretical functions for attenuations and velocities versus angle $\alpha$, and the model parameters are listed in Table 1.

The P-, SV-, and SH-wave experimental data and theoretical functions for velocities and attenuations are shown in Figs. 2 and 3, respectively. They were calculated with the use of the model-input parameters $\Delta_N^I$, $\Delta_T^I$, $\Delta_N$, $\Delta_T$, $g$ given in Table 1. This is the data obtained from the experiment with the linear acquisition system shown in Fig. 1b the compressing pressure $P = 2\,\text{MPa}$. The case of the conical acquisition system (shown in Fig. 1c) was considered by Chichinina et al. (2007a,b).

**Table 1** Model-input parameters used for numerical modeling

| Model | $\Delta_N$ | $\Delta_T$ | $\Delta_N^I$ | $\Delta_T^I$ | $g$ | $V_P$ (m/s) | $V_S$ (m/s) | $Q_b^{-1}$ |
|---|---|---|---|---|---|---|---|---|
| Wet | 0.28 | 0.15 | 0.134 | 0.087 | 0.218 | 2,786 | 1,300 | 0.047 |
| Dry | 0.63 | 0.56 | 0.110 | 0.010 | 0.218 | 2,786 | 1,300 | 0.031 |

*Note.* $Q_b^{-1}$ is the S-wave attenuation in background material (see Eq. 11); it was estimated to be the SH-wave attenuation measured at $\alpha = 90°$

## 5 Numerical Modeling and the Laboratory Experiment

Figure 2 shows P- and SH-wave velocities, obtained in the experiment, and theoretical velocity functions $V_P(\alpha)$, $V_{SV}(\alpha)$, $V_{SH}(\alpha)$, calculated from Eqs. 5 to 7 as real parts of complex-valued velocities $\tilde{V}_m(\alpha)$, m=P, SV, SH. The normal weakness $\Delta_N$ in the dry model is greater than in the oil-saturated model, because dry fractures decrease the total stiffness more than wet factures. Therefore the P-wave velocity in the oil-saturated model is greater than in the dry model. The velocity anisotropy in dry model is stronger than in saturated model. This is in accordance with the experiment of Hsu and Schoenberg (1993) and Schoenberg's LS theory (see also Bakulin et al. 2000).

Figure 3 shows the P-, SV-, and SH-wave attenuations for the experimental data and the theoretical functions $Q_P^{-1}(\alpha)$, $Q_{SV}^{-1}(\alpha)$, and $Q_{SH}^{-1}(\alpha)$, in accordance with Eqs. 8–10. The velocity and attenuation functions, $V(\alpha)$ and $Q^{-1}(\alpha)$, exhibit similar patterns, but the behavior of the attenuation function is reciprocal to the velocity function, following the principle that "the maximum of the velocity curve corresponds to the minimum of the attenuation curve, and vice versa." Both P-wave anisotropies—of velocity and attenuation—are greater in the dry model than in the saturated model. The attenuation anisotropy is much greater than the velocity anisotropy. The P-wave velocity anisotropy is 10–38% but attenuation anisotropy is substantially larger, 114–153%, where the attenuation anisotropy is 2(max−min)/(max+min). This suggests that even when the velocity anisotropy is small, there may still be a strong attenuation anisotropy.

Surface seismic reflection data and vertical seismic profiling (VSP) data deal with the wave-incidence angles from 0° to 40°. In this interval, as is clearly seen in Fig. 2, in the dry model, the P-wave velocity is much lower than in the wet model; the S-wave velocities in the dry model also are lower than those in the wet model, but the percentage decrease is less than that for P-wave. Looking at Fig. 3, we see that in the dry model, in the interval (0°–40°), P-wave attenuation is much greater than attenuations of waves SV and SH. In the oil-saturated model, on the contrary, all three attenuations are similar.

## 6 Attenuation Anisotropy in Dry and Saturated Models

In surface seismic reflection data and VSPs, wave-incidence angles are from 0° to 40°. In Fig. 3, it is clearly seen that in the dry model, in this interval, i.e., in the vicinity of the point $\alpha = 0°$, P-wave attenuation is much greater than attenuations of waves SV and SH. In the oil-saturated model, on the contrary, all three functions are similar, with attenuation for the P-wave slightly larger than that for S-waves (although it should be noted that the relationship between P- and S- attenuations may be opposite in oil-saturated models, as observed by Gik and Bobrov (1996) in the experiment with compressing pressure $P = 4$ MPa). Data on P- and SH-wave attenuation obtained at $P = 4$ MPa are presented in Fig. 4, together with

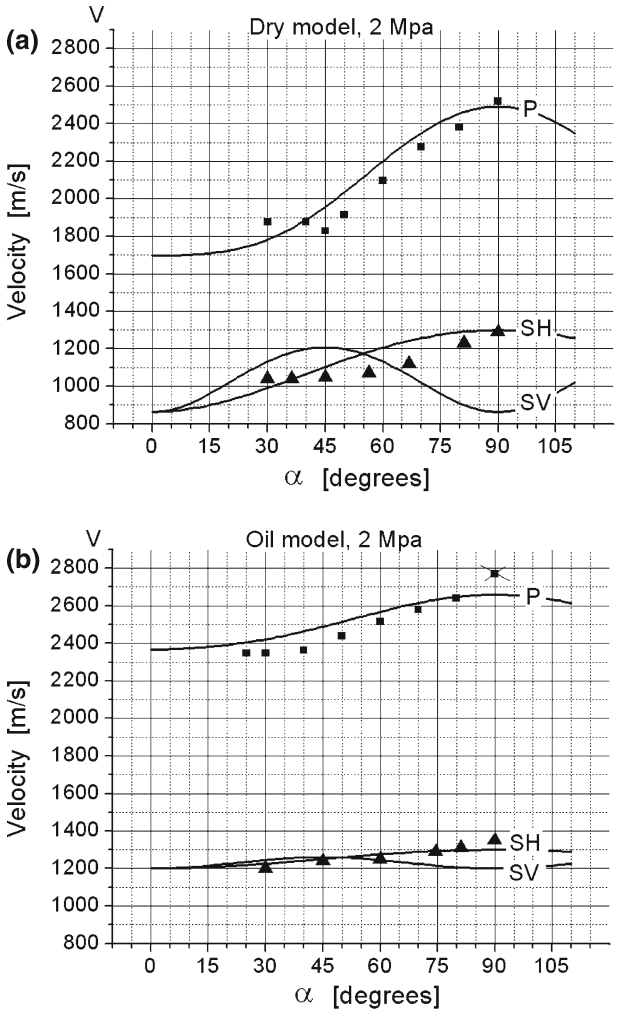


**Fig. 2** The velocity data (marked by symbols) and the theoretical curves $V(\alpha)$ for the P-, SV-, and SH-wave velocities in the dry model (**a**) and the oil-saturated model (**b**). The angle $\alpha$ is measured as the angle between the ray and the symmetry axis. The velocity values marked by symbols are the experimental data from Gik and Bobrov (1996). The solid lines are velocity functions $V(\alpha)$ calculated from Eqs. 5 to 7 with the model-input parameters given in Table 1

the data for $P = 2$ MPa (the latter are shown in more detail in Fig. 3). Figure 4 illustrates the influence of a compressing pressure on an anisotropy strength and a behavior of dependences $Q_{\mathrm{P}}^{-1}(\alpha)$, $Q_{\mathrm{SH}}^{-1}(\alpha)$. As would be expected, the increase of the pressure $P$, from 2 to 4 MPa, leads to a general decrease in attenuation anisotropy. In Fig. 4 for the cases $P = 2$ MPa and $P = 4$ MPa, the relative positions of the P- and SH-wave attenuation curves differ in the dry and the oil-saturated models. The dry model is characterized by great contrast between the curves, namely, $Q_{P\perp}^{-1} \gg Q_{S\perp}^{-1}$; it is seen in the vicinity of $\alpha = 0°$ indicated as "$\perp$ direction". The distinction between the P- and SH-wave curves extends the whole $\alpha$-range (0°, 90°) for the dry model. While in the saturated model, the contrast is insignificant, $Q_{P\perp}^{-1}/Q_{S\perp}^{-1} \cong 1$ Symbols $\perp$ and $\parallel$ denote directions perpendicular and parallel to fracture planes, respectively.

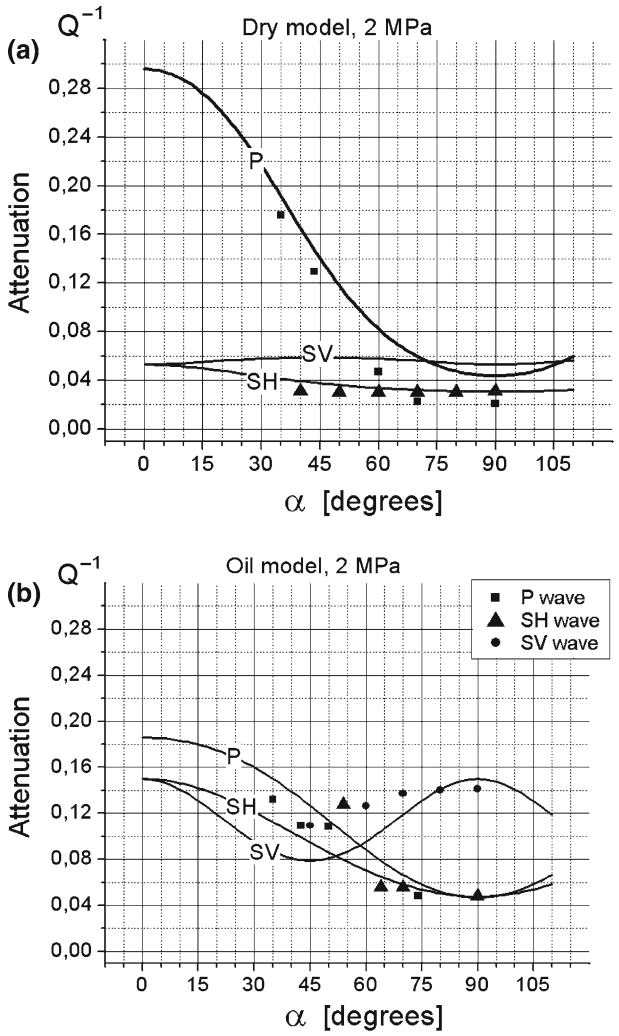


**Fig. 3** The experimental attenuation data (marked by symbols) and the theoretical curves $Q^{-1}(\alpha)$ for the P-, SV- and SH-wave attenuation in the dry model (**a**) and the oil-saturated model (**b**). The experimental values are from Gik and Bobrov (1996), the theoretical curves $Q^{-1}(\alpha)$ are calculated from Eqs. 8 to 10 with the model-input parameters given in Table 1

Thus, the data presented in Fig. 4 confirm a known result on correlation $Q_P^{-1}$ with $Q_S^{-1}$, following which liquid-saturated rocks exhibit the P-wave attenuation roughly equal to the S-wave attenuation, while in gas-saturated rocks (in our case—in the dry model), P-wave attenuation is greater than S-wave attenuation (Klimentos 1995; Dvorkin and Mavko 2006). We assume our dry model (which is actually air-filled) is a model of a gas-saturated rock, because the ultrasonic experiment of Toksöz et al. (1979) demonstrates that dry and methane-saturated rocks exhibited similar attenuation properties.

Because P-wave data are commonly used in seismic exploration, we seek to find attributes of P-wave attenuation $Q_P^{-1}(\alpha)$, $\alpha \cong 0$–$40°$, that enable differentiation of the fracture fluid fill.

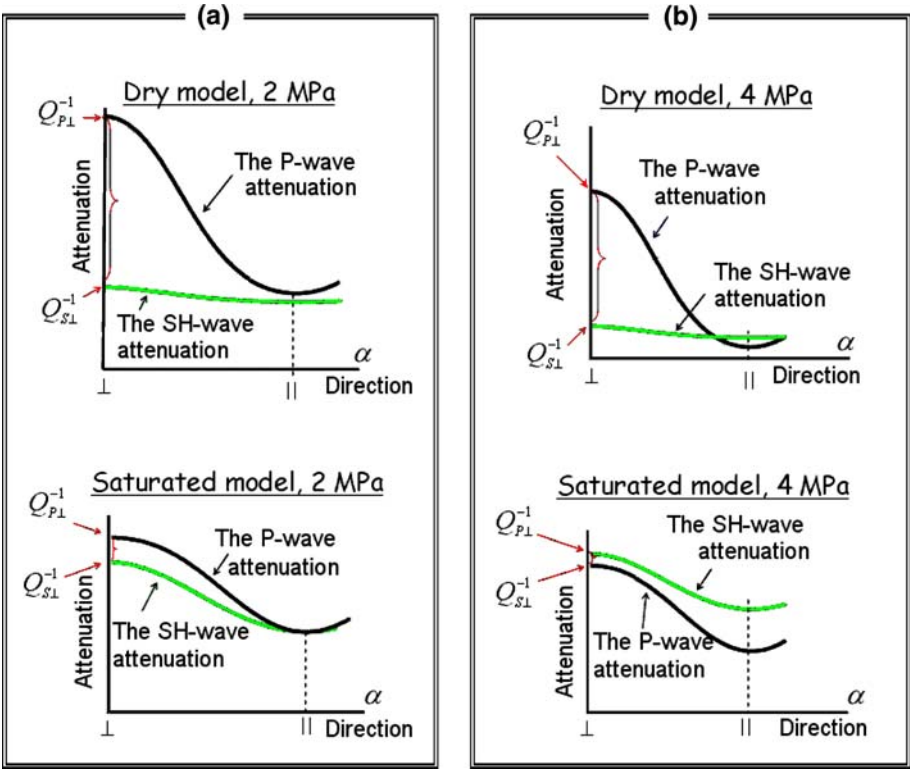


**Fig. 4** Comparison of the P-wave attenuation and the SH-wave attenuation for the dry and saturated models in the cases of compressing pressure of 2 MPa (**a**) and 4 MPa (**b**). The presented curves are theoretical ones calculated from Eqs. 8 to 10 with the model-input parameters derived from the data of Gik and Bobrov (1996)

It readily follows from comparison of initial parts of the curves $Q_{\mathrm{P}}^{-1}(\alpha)$ in Fig. 4 for the dry and oil-saturated models and from the linear approximation for $Q_{\mathrm{P}}^{-1}(\alpha)$, Eq. 12, that the coefficient $B$ is the sought-after attribute. It is illustrated by Fig. 5, which shows a steeper slope for the linear fit, $Q_{\mathrm{P}}^{-1}(x) = A + Bx$, $x = \sin^2\alpha$, of the dry model than of the oil-saturated one ($P = 2$ MPa). We name the coefficient $B$ as the QVO gradient, and $A$ as the QVO intercept (or vertical attenuation). The QVO gradient and the intercept are introduced exactly in the same manner as the AVO gradient and the intercept in the AVO analysis.

The significance of the QVO gradient lies also in its connection with a curvature of the attenuation function $Q_{\mathrm{P}}^{-1}(\alpha)$ at $\alpha = 0°$, i.e.,

$$2B = \partial^2 Q_{\mathrm{P}}^{-1}/\partial\alpha^2\Big|_{\alpha=0}. \tag{17}$$

For the normalized QVO gradient, i.e., $B/A$, according to Eq. 13, we derived the following relation (Chichinina et al. 2007a,b):

$$B/A = 4\left(Q_{\mathrm{S}\perp}^{-1}/Q_{\mathrm{P}\perp}^{-1} - 1\right)\,(V_{\mathrm{S}\perp}/V_{\mathrm{P}\perp})^2, \tag{18}$$

where $Q_{\mathrm{P}\perp}^{-1}$, $Q_{\mathrm{S}\perp}^{-1}$,$V_{\mathrm{P}\perp}$, and $V_{\mathrm{S}\perp}$ are the symmetry-axis P- and S-wave attenuations and velocities. Eq. 18 becomes simple for the case $V_{\mathrm{S}\perp}/V_{\mathrm{P}\perp} = 0.5$, which yields the following concise expression:

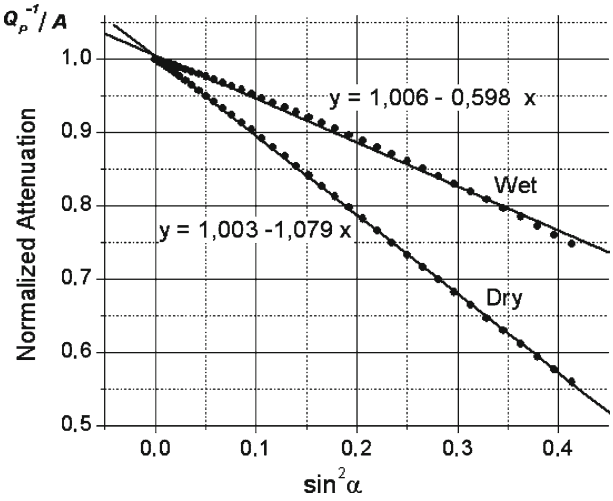


**Fig. 5** Synthetic data (marked by dots) and the linear fit $y = a + bx$ (solid line) for wet and dry models. The axes are $x \equiv \sin^2\alpha$ and $y \equiv (Q_{\mathrm{P}}^{-1}(\alpha)/A)$, where $A$ is the vertical attenuation

$$B/A = \left(Q_{\mathrm{S}\perp}^{-1} - Q_{\mathrm{P}\perp}^{-1}\right)/Q_{\mathrm{P}\perp}^{-1}. \tag{19}$$

It follows that this describes the normalized QVO gradient: it is the relative difference between the symmetry-axis S- and P-wave attenuations. Thus, the more the absolute difference between $Q_{\mathrm{S}\perp}^{-1}$ and $Q_{\mathrm{P}\perp}^{-1}$, the greater the absolute value of $B/A$. In the case of the dry model, the difference $\left|Q_{\mathrm{S}\perp}^{-1} - Q_{\mathrm{P}\perp}^{-1}\right|$ is greater than that in the saturated model, and therefore, the absolute value of the QVO gradient is greater. We confirmed this with ultrasonic experiment data.

Following the QVO-gradient definition as the second derivative of $Q_{\mathrm{P}}^{-1}(\alpha)$, Eq. 17, the normalized QVO gradient, $B/A$, is equal to Thomsen-style attenuation parameter $\delta_{\mathrm{Q}}$, which is involved in the approximation Zhu and Tsvankin (2006),

$$Q_P^{-1} = Q_{P\perp}^{-1}(1 + \delta_{\mathrm{Q}} \sin^2\alpha + (\varepsilon_{\mathrm{Q}} - \delta_{\mathrm{Q}}) \sin^4\alpha), \tag{20}$$

which is analogous to the three-term approximation (16). Thomsen-style attenuation parameter $\varepsilon_{\mathrm{Q}}$ is independent of the attenuation properties due to fractures, because $\varepsilon_{\mathrm{Q}}$ is a simple function of $V_{\mathrm{P}}/V_{\mathrm{S}}$-ratio of the background and the normal weakness $\Delta_{\mathrm{N}}$ (Chichinina et al. 2007a,b):

$$\varepsilon_{\mathrm{Q}} = \frac{-4g(1-g)}{1 - \Delta_{\mathrm{N}}(1-2g)^2}. \tag{21}$$

However, the parameter $\delta_{\mathrm{Q}}$ may be meaningful for fracture characterization, because it can be defined by the symmetry axis $Q_{\mathrm{P}\perp}/Q_{\mathrm{S}\perp}$-ratio, following Eq. 18, where $B/A = \delta_{\mathrm{Q}}$.

## 7 QVO Gradient for Wet and Dry Models

Figure 5 shows the QVO response (normalized P-wave attenuation versus $\sin^2\alpha$) in wet and dry models. The range of the incidence angles $\alpha$ from 0° to 40° is considered in the reflection

data. Figure 5 plots synthetic data (marked by dots) generated by Eq. 8 for $Q_{\mathrm{P}}^{-1}(\alpha)$, with the parameters given in Table 1.

We assume that in real reflection data, $Q_{\mathrm{P}}^{-1}(\alpha)$ can be estimated from pre-stack reflection data as $Q^{-1}$ versus offset. Note that for better visual demonstration, we plot $Q_{\mathrm{P}}^{-1}(\alpha)$ divided by the vertical attenuation $A$. A linear function $y = a + bx, x = \sin^2\alpha$ (drawn by solid line), was least-squares fit, as is commonly used in the AVO method. The formulae of the linear fit are given within the plot, for dry and oil-saturated models. Following the linear approximation (12), the coefficient $b$ plays the part of the normalized QVO gradient, $b = B/A$, and the coefficient $a$ is the normalized intercept, $a = A/A = 1$. Following Eq. 18, the absolute value of the normalized QVO gradient $B/A$ should be greater in the dry model than in the wet model, because $\left|Q_{\mathrm{S}\perp}^{-1} - Q_{\mathrm{P}\perp}^{-1}\right|$ is greater in the dry model than in the wet model. This is confirmed by the numerical modeling, which yields $|b| = 1.079$ for the dry model, and $|b| = 0.598$ for the wet model.

Let us consider an analogy between QVO and AVO. In AVO analysis, the difference in $V_{\mathrm{S}}/V_{\mathrm{P}}$-ratios (or Poisson's ratios) in liquid-saturated and gas-saturated rocks acts to produce different offset responses (Castagna 1993). Being linked to the $V_{\mathrm{S}}/V_{\mathrm{P}}$-ratio, the AVO gradient is greater in gas-saturated rocks than in liquid-saturated rocks. As for QVO, the QVO gradient is linked to $Q_{\mathrm{S}}/Q_{\mathrm{P}}$-ratio, which is different in liquid-saturated and gas-saturated rocks. Thus, similar to the AVO gradient, the QVO gradient is greater in gas-saturated rocks than in liquid-saturated rocks.

## 8 Discussion and Conclusions

Comparison between the laboratory-experiment data and the theory-predicted variations of velocities and attenuations provides a support for consistency of the developed theoretical model. The attenuation anisotropy and the velocity anisotropy are interlinked. They are interlinked by the parameters $\Delta_{\mathrm{N}}$, $\Delta_{\mathrm{T}}$, and $g(g = (V_{\mathrm{S}}/V_{\mathrm{P}})^2)$. We fitted the experimental data with theoretical functions and demonstrated the validity of the theoretical model. The velocity and attenuation functions exhibit similar patterns, but the behavior of the attenuation function is reciprocal to the velocity function, in accordance with the principle "the maximum of velocity curve corresponds to the minimum of attenuation curve, and vice versa". The attenuation anisotropy is much greater than the velocity anisotropy. The variations measured in the experiment show the P-wave velocity anisotropy of 10–38%, but is substantially stronger in the attenuation anisotropy (114–153%). This suggests that even when the velocity anisotropy is small, there may still be a strong attenuation anisotropy.

We confirm a known result from rock physics and well-log analysis that $Q_{\mathrm{S}}/Q_{\mathrm{P}} \cong 1$ in liquid-saturated rocks, and $Q_{\mathrm{S}}/Q_{\mathrm{P}} > 1$ in gas-saturated rocks (Klimentos 1995; Dvorkin and Mavko 2006). This was confirmed by the numerical modeling based on the experimental data. In the wet (oil-saturated) model, the symmetry-axis P-wave attenuation is close to the symmetry-axis S-wave attenuation, while in the dry (air-saturated) model, the P-wave attenuation becomes much greater than S-wave attenuation. We also have found out that the fluid fill should affect the P-wave attenuation pattern. In dry model, the attenuation pattern should exhibit a steeper slope and curvature than in the wet model. To define the slope and the curvature, we introduce the QVO gradient, which was found to be proportional to the symmetry-axis $Q_{\mathrm{S}}/Q_{\mathrm{P}}$-ratio, and that is why it should be different across dry and wet models; the QVO gradient should be greater in gas-saturated rocks than in liquid-saturated rocks.

Thus, depending on the $Q_S/Q_P$-ratio, the QVO gradient may serve as an indicator of the crack-fill fluid. However, for reliable theory confirmation, additional experiments are needed, in which the complete angle range ($\alpha$ from 0° to 90°) should be explored.

The analysis of P-wave attenuation versus offset (QVO) is in use in seismic exploration, particularly, for distinguishing gas saturation from liquid saturation. This requires development of the QVO analysis for both HTI and VTI media. Hydrocarbon-bearing rocks of HTI type can be revealed from azimuthal variations of P-wave attenuation, and fluid in cracks can be derived by the QVO data, at least in principle. In the case of VTI media, to find hydrocarbon-bearing rocks from QVO analysis and to distinguish gas from liquid is much more difficult because of competing actions of two factors: horizontal thin-layering and horizontal fracturing, which are two different types of anisotropy in VTI media. Here, we presented the theory for an attenuative VTI LS-medium whose anisotropy was due to horizontal fracturing, which cannot be considered as a typical model for the earth structure. Next we are going to extend our approach to more realistic VTI-medium model that includes both horizontal fracturing and thin layering. The use of Schoenberg's linear-slip model (Schoenberg and Douma 1988; Schoenberg and Nakagawa 2006) will be the foundation for constructing such a model with complex-valued weaknesses.

We realize that distinction between dry and wet fractures only from attenuation anisotropy field data cannot be unambiguous. Therefore, our proposal is in joint interpretation of all available data on anisotropy in P- and S-wave velocities, attenuations, and reflection coefficients.

**Acknowledgements** We are greatly indebted to Dr Leonid Gik and Dr Boris Bobrov for their support with the data of the ultrasonic experiment, which was performed in the Institute of Petroleum Geology and Geophysics of Siberian Branch of Russian Academy of Sciences, Novosibirsk, Russia.

## References

Bakulin, A., Grechka, V., Tsvankin, I.: Estimation of fracture parameters from reflection seismic data—part I: HTI model due to a single fracture set. Geophysics **65**, 1788–1802 (2000)

Best, A.I., Sothcott, J., McCann, C.: A laboratory study of seismic velocity and attenuation anisotropy in near-surface sedimentary rocks. Geophys. Prosp. **55**, 609–625 (2007)

Carcione, J.M.: A model for seismic velocity and attenuation in petroleum source rocks. Geophysics. **65**, 1080–1092 (2000)

Castagna, J.: AVO analysis—tutorial and review. In: Castagna, J., Backus, M. (eds.) Offset Dependent Reflectivity—Theory and Practice of AVO Analysis, Soc. Expl. Geophys. pp. 3–36 (1993)

Chapman, M.: Frequency—dependent anisotropy due to meso-scale fractures in the presence of equant porosity. Geophys. Prosp. **51**, 369–379 (2003)

Chichinina, T., Sabinin, V., Ronquillo-Jarillo, G.: QVOA analysis: P-wave attenuation anisotropy for fracture characterization. Geophysics. **71**, C37–C48 (2006a)

Chichinina, T., Sabinin, V., Ronquillo-Jarillo, G., Obolentseva, I.: The QVOA method for fractured reservoir characterization. Russ. Geol. Geophys. **47**(2), 265–283 (2006b)

Chichinina, T.I., Obolentseva, I.R., Ronquillo-Jarillo, G., Sabinin, V.I., Gik, L.D., Bobrov, B.A.: Attenuation anisotropy of P- and S-waves: theory and laboratory experiment. J. Seismic Explor. **16**, 235–264 (2007a)

Chichinina, T., Ronquillo-Jarillo, G., Sabinin, V., Obolentseva, I., Gik, L., Bobrov, B.: Attenuation anisotropy linked to velocity anisotropy: theory and ultrasonic experiment. In: Expanded Abstracts of the 77th Annual International Meeting, SEG, pp. 149–153 (2007b)

Clark, R.A., Carter, A.J., Nevill, P.C., Benson, P.M.: Attenuation measurements from surface seismic data: azimuthal variation and time-lapse case studies. The EAGE 63rd Conference and Technical Exhibition, p. L28 (2001)

Crampin, S.: A review of wave motion in anisotropic and cracked elastic-media. Wave Motion. **3**, 343–391 (1981)

Domnesteanu, P., McCann, C., Sothcott, J.: Velocity anisotropy and attenuation of shale in under- and overpressured conditions. Geophys. Prosp. **50**, 487–503 (2002)
Dvorkin, J.P., Mavko, G.: Modeling attenuation in reservoir and nonreservoir rock. Lead. Edge. pp. 194–197 (2006)
Gik, L.D., Bobrov, B.A.: Experimental laboratory study of anisotropy for thin-layered media. Russ. Geol. Geophys. **37**(5), 94–107 (1996)
Hosten, B., Deschamps, M., Tittmann, B.R.: Inhomogeneous wave generation and propagation in lossy anisotropic solids: Application to the characterization of viscoelastic composite materials. J. Acoust. Soc. Am. **82**, 1763–1770 (1987)
Hudson, J.A.: Wave speeds and attenuation of elastic waves in material containing cracks. Geophys. J. Roy. Astr. Soc. **64**, 133–150 (1981)
Hudson, J.A., Liu, E., Crampin, S.: The mechanical properties of materials with interconnected cracks and pores. Geoph. J. Int. **124**, 105–112 (1996)
Hudson, J.A., Pointer, T., Liu, E.: Effective-medium theories for fluid-saturated materials with aligned cracks. Geophys. Prosp. **49**, 509–522 (2001)
Hsu, C.-J., Schoenberg, M.: Elastic waves through a simulated fractured medium. Geophysics **58**, 964–977 (1993)
Klimentos, T.: Attenuation of P- and S-waves as a method of distinguishing gas and condensate from oil and water. Geophysics. **60**, 447–458 (1995)
Liu, E., Crampin, S., Queens, J.H., Rizer, W.D.: Velocity and attenuation anisotropy caused by microcracks and macrofractures in a multiazimuth reverse VSP. Can. J. Explor. Geophys. **29**(1), 177–188 (1993)
Liu, E., Chapman, M., Varela, I., Li, X.-Y., Queen, J.H., Lynn, H.: Velocity and attenuation anisotropy: implication of seismic fracture characterizations. Lead. Edge **26**, 1170–1174 (2007)
MacBeth, C.: Azimuthal variation in P-wave signatures due to fluid flow. Geophysics. **64**, 1181–1192 (1999)
Maultzsch, S., Chapman, M., Liu, E., Li, X.-Y.: Modeling and analysis of attenuation anisotropy in multi-azimuth VSP data from the Clair field. Geophys. Prosp. **55**, 627–642 (2007)
Schoenberg, M.: Elastic wave behavior across linear slip interfaces. J. Acoust. Soc. Am. **68**, 1516–1521 (1980)
Schoenberg, M.: Reflection of elastic waves from periodically stratified media with inter-facial slip. Geophys. Prosp. **31**, 265–292 (1983)
Schoenberg, M., Douma, J.: Elastic wave propagation in media with parallel fractures and aligned cracks. Geophys. Prosp. **36**, 571–590 (1988)
Schoenberg, M., Sayers, C.M.: Seismic anisotropy of fractured rock. Geophysics. **60**, 204–211 (1995)
Schoenberg, M., Nakagawa, S.: Soft layers, fractures and anisotropy. In: 68th EAGE Conference & Exhibition, Proceedings of the Workshop on Seismic Anisotropy—State of the Art in Parameter Estimation and Imaging, pp. 23–26 (2006)
Shi, G., Deng, J.: The attenuation anisotropy of mudstones and shales in subsurface formations. Sci. China, Ser. D (Earth Sci). **48**(11), 1882–1890 (2005)
Sothcott, J., Best, A.I., McCann, C.: Laboratory characterization of porous, permeable media with aligned penny shaped cracks at ultrasonic frequencies. The 69th EAGE Conference, London, Paper F013 (2007)
Toksöz, M.N., Johnston, D.H., Timur, A.: Attenuation of seismic waves in dry and saturated rocks: I. Lab. Meas. Geophys. **41**, 681–690 (1979)
Varela, I., Nasser, M., Chapman, M., Liu, E.: Anisotropic azimuthal attenuation as an indicator of fracture properties, a case study on time-lapse walkaround VSP data. The EAGE 68th Conference and Technical Exhibition, Vienna, Paper P146 (2006)
Vasconcelos, I., Jenner, E.: Estimation of azimuthally varying attenuation from wide-azimuth P-wave data. Expanded Abstracts of the 75th Annual International Meeting, Soc. Expl. Geophys. (2005)
Zhu, Y., Tsvankin, I.: Plane-wave propagation in attenuative transversely isotropic media. Geophysics. **71**, T17–T30 (2006)
Zhu, Y., Tsvankin, I., Dewangan, P., van Wijk, K.: Physical modeling and analysis of P-wave attenuation anisotropy in transversely isotropic media. Geophysics. **72**, D1–D7 (2007)